Image analysis of epicuticular damage to foliage caused by dry deposition of the air pollutant nitric acid

Pamela E. Padgett,*[a] Sally D. Parry,[b] Andrzej Bytnerowicz[a] and Robert L. Heath[b]

Received 26th March 2008, Accepted 17th September 2008
First published as an Advance Article on the web 23rd October 2008
DOI: 10.1039/b804875d

Nitric acid vapor is produced by the same photochemical processes that produce ozone. In the laboratory, concentrated nitric acid is a strong acid and a powerful oxidant. In the environment, where the concentrations are much lower, it is an innocuous source of plant nitrogen. As an air pollutant, which mode of action does dry deposition of nitric acid follow? We investigated the effects of dry deposition of nitric acid on the foliage of four tree species native to the western United States. A novel controlled environment, fumigation system enabled a four-week exposure at concentrations consistent with ambient diurnal patterns. Scanning electron microscopy and automated image analysis revealed changes in the epicuticular wax layer during fumigation. Exposure to nitric acid resulted in a reproducible suite of damage symptoms that increased with increasing dose. Each tree species tested exhibited a unique set of damage features, including cracks, lesions, and conformation changes to epicuticular crystallite structures. Dry deposition of atmospheric nitric acid caused substantial perturbation to the epicuticular surface of all four tree species investigated, consistent with the chemical oxidation of epicuticular waxes. Automated image analysis eliminated many biases that can trouble microscopy studies. Trade names and commercial enterprises or products are mentioned solely for information. No endorsements by the U.S. Department of Agriculture are implied.

Introduction

Nitric acid (HNO_3) is a secondary urban air pollutant produced during the same photochemical processes that produce ozone (O_3).[1] Unlike O_3 once created, HNO_3 no longer participates in atmospheric gaseous reactions, but is highly reactive with aqueous and solid substrates. In nature, at low concentrations, HNO_3 and its associated anion, nitrate (NO_3^-), are relatively innocuous, being a primary source of the plant nutrient nitrogen. Under more concentrated conditions, however, HNO_3 is a strong acid and powerful oxidant used in a wide variety of organic reactions. The question arises whether the deposition of the atmospheric pollutant HNO_3 on plant leaves follows a model in keeping with its non-phytotoxic behavior as a plant nutrient, or whether its activity is more in keeping with its behavior as a strong acid and oxidizer.

The photochemical reactions that create atmospheric HNO_3 are fairly well understood.[1] However, real-time concentrations are not well established because of instrument limitations. Speculation based on principles of atmospheric chemistry has maintained that diurnal patterns of HNO_3 synthesis should parallel those of O_3, since both are formed photochemically. Nitric acid concentrations are expected to be close to zero during dark hours, build during daylight hours to reach a peak sometime in the afternoon, and decline with sunset. Recent work by Furutani and Akimoto[2] using chemical ionization mass spectrometry (CIMS) have provided empirical data in support of this proposed diurnal pattern. Prior to CIMS, denuder methods provided the most reliable measurements of ambient HNO_3 concentrations,[3,4] but these measurements are typically 12 to 24 h integrated determinations. Twelve-hour concentrations greater than 2.5 μg m^{-3} or 24 h concentrations greater than 5.1 μg m^{-3} are considered elevated pollutant loads,[5] but no concentration standards exist in the United States. In southern California, daytime 12 h average concentrations up to 46.7 μg m^{-3} have been reported.[6]

The level of NO_3^- in rainwater can range from 30 to 40 μeq L^{-1}.[7] Concentrations in fog can reach much higher levels. Fenn *et al.*[8] measured fog concentrations of 324 μeq L^{-1} in southern California. In arid and semi-arid environments, HNO_3 is deposited largely in dry form, either as particulates or in molecular form. Dry deposition at low elevations in southern California may account for 95% of the total terrestrial load of nitrogen (N), at 35 to 50 kg ha^{-1} annually.[9,10] In more temperate climates, dry deposition accounts for 30% to 50% of the total deposition load.[11,12] Leaf-wash and throughfall studies use the accumulation of NO_3^- on foliage to estimate total dry deposition loads.[13–15] Dry deposition concentrations of N have been reported to range from 1.0 to 2.5 μg cm^{-2} on pine needles.[15] Assuming a water-saturated boundary layer around the leaf of less than 0.1 mm deep, 2.5 μg N cm^{-2} from NO_3^- on a leaf surface would approach an aqueous concentration of 10 eq L^{-1}. This theoretical aqueous concentration is several orders of magnitude higher than the most concentrated wet deposition reported in recent literature.[1] The direct effect of very high HNO_3 concentrations due to dry deposition on surfaces of living foliage has not been established.[16]

[a]*Riverside Fire Laboratory, USDA Forest Service, Riverside, CA, 92507. E-mail: ppadgett@fs.fed.us; Fax: +1 951 680 1501; Tel: +1 951 680 1584*
[b]*Department of Botany and Plant Sciences, University of California, Riverside, CA, 92521*

Our preliminary studies involving 24 or 48 h continuous fumigation of *Quercus kelloggii* Newb. (California black oak) and *Pinus ponderosa* Laws. (ponderosa pine) at 50 ppb (w/v) (141 $\mu g\ m^{-3}$) to 200 ppb (575 $\mu g\ m^{-3}$) HNO_3 showed perturbations to the foliar surface, including cuticular lesions and disruption of the stomatal chamber.[16,17] These studies involved the use of an older fumigation system that could not reproduce known patterns of ambient conditions. The observations, however, were compelling enough to prompt development of an improved fumigation system that allowed more detailed investigations of foliar responses to dry deposition.[18]

All terrestrial leaf cuticles are coated with a layer of lipids and waxes. The exact chemical composition of these epicuticular waxes is species-dependent and can be influenced by environmental conditions.[19–21] The epicuticular waxes form a barrier between the largely aqueous internal environment and the desiccating external environment. They provide protection from water, nutrient, and metabolite losses, as well as a barrier to environmental toxins and infection by pathogens. The synthesis of waxes occur in the epidermal cells, but the mechanisms for transport of waxes or their precursors to the surface and the formation of the final crystalline structures are largely unknown.[22–24] In general, once waxes are deposited on the leaf surfaces and the leaves are fully expanded, plants do not repair damage done to the cuticle, but exceptions occur.

Damage to the epicuticular layer from air pollutants has been investigated in controlled experimental and field studies. Ozone, acid rain, and deposited particulates are known to cause damage to the epicuticular surface of plant foliage. Observed damage has been reported as occlusion of stomatal cavities (particularly in the case of O_3), erosion of waxy surfaces, and accelerated aging of the foliage surface.[25–30] Because of the potential chemical reactivity of concentrated HNO_3, its effects may be particularly deleterious. The esters, primary and secondary alcohols, aldehydes, and fatty acids that make up the epicuticular waxes are subject to chemical attack and structural modification by HNO_3.[31] Epicuticular wax recrystallization experiments have demonstrated that the physical conformation of wax crystallites is dependent on their chemical structure, so a change in the chemistry alters the physical structure.[32,33]

Physical changes to the epicuticular barrier could compromise the integrity of the outer barrier, leaving foliage vulnerable to desiccation, nutrient loss and pest attack,[34] or exacerbate the effects of other environmental pollutants.[26] Therefore, the seasonal effects of dry deposition of HNO_3 may have subtle, but cumulative, consequences on survival during periods of stress.

Several studies have investigated the effects of air pollutants on the cuticular surfaces of leaves and identified symptoms induced by a specific treatment or deduced cause and effect by pollution with use of environmental measures.[35] In most cases, leaf samples are examined carefully, and features that are consistent with an external environmental factor are recorded and analysed. An alternative approach is to select samples randomly from leaves and needles without prior examination, create images of those samples, and then subject the images to an automated analysis system.

We hypothesized that dry HNO_3 deposition attacks and damages the epicuticular waxes of foliage, consistent with the behavior of concentrated acids and oxidants. Using a controlled environment fumigation system, we exposed seedlings of four tree species native to the western US to zero, moderate and high levels of HNO_3 vapor, and used SEM to examine changes induced in the epicuticular wax layer. Over 1,200 SEM images were captured from random locations on foliage samples, and image analysis techniques were used methodically to evaluate and quantify changes to the epicuticular surface.

Experimental

Plant material

We chose species native to the mixed conifer forests of the western United States, which is experiencing increased pressure from anthropogenic disturbances including air pollution.[9] Ponderosa pine (*Pinus ponderosa*, Laws.) is the best-studied species of the group and is often dominant in the forest community. White fir (*Abies concolor*, Lindley) is a shade-tolerant species that seems to be thriving where fire has been suppressed and often forms dense thickets. California black oak (*Quercus kelloggii*, Newb.) is a deciduous oak species important as a food source and nesting site for wildlife. It is often an understory species in mixed conifer forests or in homogeneous stands of oak woodland. Canyon live oak (*Quercus chrysolepis*, Liebm.) is among the most adaptable of the native western oaks. It can be found in mixed chaparral stands, in riparian zones, standing alone on steep hillsides or in the understory of pine forests. It is an evergreen with sclerophyllous leaves typical of chaparral species.[36]

Canyon live oak and California black oak individuals were half-siblings. Seeds of canyon live oak were collected from an isolated tree on the University of California, Riverside, (UCR) campus, and seeds of black oak were collected from an isolated tree near Running Springs in the San Bernardino Mountains. Canyon live oak and black oak plants were approximately one year old at the time of the study. Ponderosa pine individuals were purchased from the California Reforestation Nursery, Davis, CA, and white fir individuals from Cornflower Farms (Elk Grove, CA, USA) as 2 year-old plants and acclimated to the research greenhouse for three months before the study began. Trees were planted in 7 litre pulp pots (Western Pulp Products, Corvallis, OR, USA), and grown in a greenhouse at UCR, where the fumigation facility is housed. The pines, firs, and black oaks were planted in Sunshine mix #4 (Sungro Horticulture, Bellevue, WA, USA), a highly porous medium, and the canyon live oaks were planted in UC soil mix #3 (75% sand, 25% ground peat moss).

Five replicate trees in three treatments, zero, moderate and high levels of HNO_3 were evaluated. The 15 individuals of each species of comparable appearance were selected from a larger grouping of plants and randomly divided into three groups of five plants. The trees were fertilized with a general-purpose, low nitrogen fertilizer ('Cactus Juice', Security Products, Tucson AZ, USA) 7 d prior to treatment. Pines and firs were also fertilized with chelated iron (Miller Chemical and Fertilizer, Hanover PA, USA). Foliar surfaces were rinsed thoroughly with distilled water 7 d and 1 d before treatment. Two treatment levels plus a 0 HNO_3 control were used for each experiment. The data were collected from two independent experiments. The first experiment investigated the oak species, and the second tested the

conifers. The oaks were placed in the fumigation chambers on April 21 ($t = 0$). The experiment ran for 33 d, ending on May 25. The pines and firs were placed in the chambers on June 9, and the experiment ran for 32 d, ending on July 13.

Fumigation system

The continuously stirred tank reactors (CSTR), similar to those described by Heagle and Phillbeck,[37] were modified for use with HNO_3 (Fig. 1).[18] The system was located in a greenhouse and adjacent headhouse on the UCR campus and consisted of three major components: clear Teflon chambers in the greenhouse, the HNO_3 vapor volatilization system for creating and delivering HNO_3 to the chambers, and a continuous, real-time monitoring system for recording chamber concentrations during the experiment. Details of the system can be found in Padgett *et al.*[18] A brief description follows.

The Teflon chambers were 1.5 m high × 1 m in diameter. The airflow through each chamber was 1.5 exchanges per minute. The bulk greenhouse air was filtered to remove particulate matter, O_3 and external HNO_3 contamination by use of standard dust filters and permanganate-activated charcoal filters (Purolator Air Filtration, Henderson NC, USA). Light in the chambers was between 1/2 and 2/3 ambient light, as determined periodically by a photometer. Ambient temperatures in the chambers reached 32 °C during summer months and 13 °C during the early spring, which is consistent with the greenhouse temperature profiles. The average daytime relative humidity in the chambers was 23%, slightly higher than the ambient greenhouse air, typically 20% during the daylight, treatment period. The rapid exchange rate in the chambers prevented significant increases in humidity and decreases in HNO_3 concentrations during the exposure period.

For production of HNO_3 vapor, ambient air from the greenhouse was dried by a heatless air dryer and filtered through an organic scrubber, activated carbon filter and high efficiency particulate arresting (HEPA) filter. The dry, filtered air was passed through the HNO_3 volatilization chamber. The volatilization chamber was submerged in a water bath heated to 84 °C—the volatilization temperature of HNO_3. Dilute HNO_3 (10% v/v) was pumped by drops into the heated chamber, causing the HNO_3 to vaporize and water to evaporate into the dry air. A total of 1 litre of 10% HNO_3 provided enough HNO_3 vapor for a 1 month fumigation experiment. The HNO_3 vapor was injected into the bulk air stream ducts 0.5 m from the inlet in the chambers. Concentrations in each of the chambers were controlled by in-line needle valves, which regulated the flow of gaseous HNO_3. The monitoring system continuously sampled each chamber, providing real-time concentrations. The CSTR monitoring system consisted of a modified scanivalve, Nitrogen Oxide Analyzer (Monitor Labs, Englewood, CO, USA), and a datalogger (Campbell Scientific, Logan, Utah, USA). All sample lines, including an ambient greenhouse line, were purged continuously. Timers controlling the system were set to mimic typical diurnal patterns of atmospheric contamination.

The control chamber (0 μg m^{-3} HNO_3) was identical to the treatment chambers. Moderate treatments were calibrated for 30 to 60 μg m^{-3} peak HNO_3 concentrations, and high treatments were calibrated for 95 to 160 μg m^{-3} peak concentrations. A typical 7 d HNO_3 concentration sequence is displayed in Fig. 2. The calculated doses used during the experiment are shown in Table 1. The 24 h averages from the moderate concentrations were consistent with typical summer concentrations in southern California. The high concentrations represented a high ambient concentration that occurs periodically in California.

Preliminary experiments

We performed a series of preliminary experiments to establish experimental protocols such as number of replicates, sampling procedure, sampling schedule and intensity, and protocols for the SEM evaluation. These experiments also investigated the potential for artifacts due to manipulation of the samples and dehydration during transport, sample preparation, and SEM. The final protocols are the result of combined experience gained from preliminary experiments and requirements of the experiment.

Sample preparation

The current year's leaf and needle samples were fully expanded prior to exposure and analysis. One leaf sample from each of the five replicate individuals was collected. Oak leaves were collected on days 0, 13, 20, 27, and 33, and conifer leaves were collected on days 0, 12, 19, 26, and 32. Sampling was skewed toward the latter half of the experiment because visible symptoms did not appear within the first two weeks, but once symptoms occurred, the progression was rapid. We collected one 6 mm diameter leaf punch from one leaf of each oak specimen. Punches were taken from the approximate center of the leaf, avoiding the mid-rib and

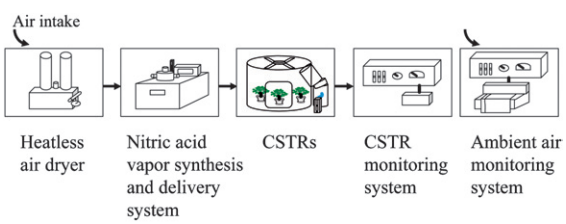

Fig. 1 Diagram of the HNO_3 fumigation system. The CSTRs are housed in a greenhouse and all other components are installed in the adjacent head house.

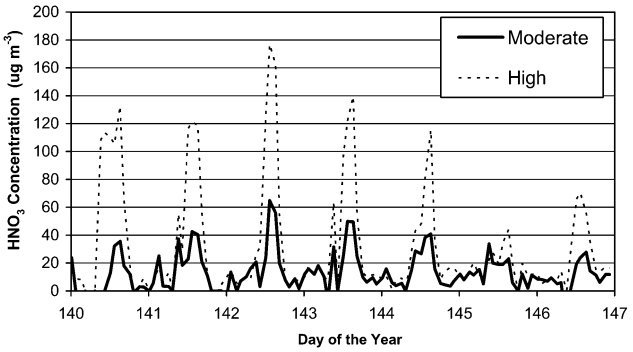

Fig. 2 A typical 7 day profile of HNO_3 concentrations during the exposures. Peak concentrations varied across days primarily in response to air temperatures in the greenhouse.

Table 1 Twenty four hour integrated average HNO_3 concentrations in chambers, and the average of the top 10% peak HNO_3 values. Data were collected in real time using a nitrogen oxide monitor. Twenty four hour exposures were calculated by integration of the continous monitoring data. Data are presented for comparison with existing ambient concentrations (*i.e.* ref. 9)

		Integrated avg. HNO_3/μg m^{-3}		Avg. peak HNO_3 (UG M-3) top 10%	
Experiment	Sample period/date	Moderate	High	Moderate	High
Oaks	1/Apr 21–May 3	13.19	18.55	90.13	123.78
	2/May 4–11	12.80	28.24	55.07	133.35
	3/May 12–18	5.05	17.51	36.64	89.13
	4/May 19–25	11.56	26.92	77.08	150.84
	1–4/Apr 21–May 25	10.65	22.81	64.73	124.27
Conifers	1/June 9–21	17.63	32.01	58.04	122.45
	2/June 22–28	12.59	18.89	40.93	74.13
	3/June 29–July 5	16.62	24.68	51.85	89.14
	4/July 6–12	15.53	41.57	39.37	154.63
	1–4/June 9–July 12	15.60	29.29	47.55	110.09

major veins. Each punch was cut in half for separate analysis of the abaxial (lower) and adaxial (upper) surfaces. We collected one 10 mm segment from the center of a one needle of each conifer specimen. Each segment was cut in half for separate analysis of the adaxial and abaxial surfaces. Pine needles are nearly triangular in cross section. The upper surface is slightly convex, whereas the lower surface has a prominent midrib giving it a v-shaped profile.

Samples were examined with an XL30-FEG scanning electron microscope (Philips, New York, NY, USA) that uses a field emission electron gun with a Schottky emission cathode. For recording the SEM images, 10 oak leaf half-punches or 15 conifer needle sections were mounted on a 32 mm diameter aluminium sample holder. Samples were affixed to mounts with a glue consisting of 4.0 mL clear nail polish, 0.5 gm finely ground spectrographic grade carbon (Ted Pella, Redding, CA, USA), and one drop of colloidal graphite in isopropanol (Ted Pella). Prepared samples were sputter coated with gold and palladium with use of an Emscope Sputter Coater 500A (Quorum Technologies, Newhaven, UK). Samples were placed approximately 40 mm from the target material (cathode) and coated at a deposition rate of 15 to 18 mA for 105 s.

To prevent data bias, samples were not previewed, but the approximate center of each sample was located, and images at 500× and 1000× magnification were recorded without prior examination. Each image was labeled with the tree number and leaf side, then stored by the date the image was taken. The images were later analysed with no foreknowledge of treatment.

Image processing for analysis

Electronic images were prepared for analysis in Photoshop 5.0 (Adobe Systems, USA). A section (Fig. 3B) was cropped from the center of the original image (Fig. 3A). Obvious nondamage-related features such as stomata, trichomes, and unusually pronounced grooves on the leaf surface were cropped out of each image (Fig. 3C). The remaining image sections were pasted together and cropped into a rectangle. Image contrast and

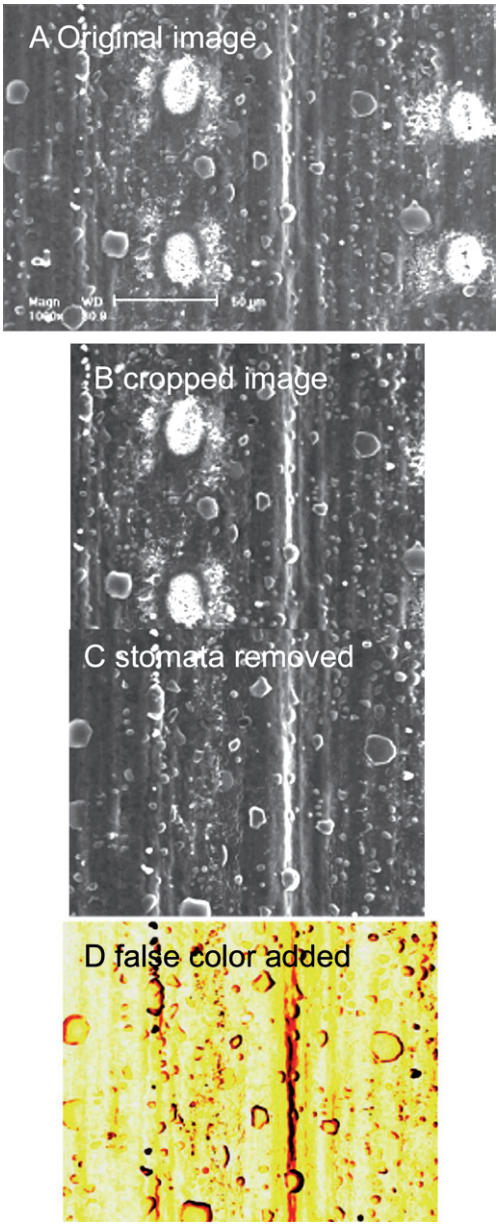

Fig. 3 Processing of images prior to image analysis. (A) Original image; (B) cropped image and the identification of feature to be eliminated; (C) final modified image; (D) application of false color.

brightness varied widely because of variation in SEM configuration during the experiment, differences in electron reflectance among species, and specimen charging effects. We visually assessed contrast and brightness for each image, and levels were adjusted accordingly. A color filter ('fire-1', inverted) from the Photoshop pallet was applied to each image, an action that increased contrast and added false color (Fig. 3D). The 'density slice' option was used to highlight damage further before analysis. The 'smooth' process, which gives the highlighted sections a clean, defined appearance, was applied to each image once. Image width and height were recorded in pixels. The final size of each processed image was adjusted so that all images were similar in size and pixel number.

Image analysis

Images were analysed by NIH Image (National Institutes of Health, USA), which allows the user to select the range of pixels included in a feature (*e.g.*, a particle). Before the feature is selected by the program, the number of pixels in that feature were counted. The particle range in the number of pixels was determined empirically by estimating the average pixel number for the damaged area on the leaf for each species. For each species, several ranges were tested, and the range that produced the highest count on images that contained damaged areas while maintaining a low count on controls was selected. For ponderosa pine 500× images, we counted particles of 5 to 300 pixels and for 1000× images, particles of 5 to 1000 pixels. For white fir, we counted particles of 200 to 1000 pixels; for black oak adaxial 500× images, particles of 50 to 500 pixels; black oak adaxial 1000× images, particles of 200 to 500 pixels. For the abaxial black oak, we applied the 'find edges' process and counted particles of 30 to 500 pixels. For canyon live oak adaxial leaf images, we counted particles of 100–500 pixels and for abaxial leaf images, particles of 100–1000 pixels. Particles touching the edge of the image were ignored. The total number of pixels in particles of the appropriate size was recorded for each image.

A damage index (DI) was calculated for each image. The DI was the ratio of the number of pixels counted in the damage features to the total number of pixels in the image. The image size was adjusted prior to analysis so that all images were of a similar size.

Experimental design and data analysis

The experiment was conducted in a controlled environment by a completely randomized design as describe by Potvin.[48] Each CSTR chamber was analysed as an independent treatment as is typical of chamber studies since true replication across chambers is rare.[49] The experimental units were individual trees and each species was replicated five times within each of the treatment chambers. Strictly speaking, the analysis can only separate differences among the chambers as the treatments themselves were not replicated. However, 30 years of research conducted in fumigation chambers have shown that the assumption that the differences among chambers are due to the imposed treatments is reasonable.[49]

The effects of treatment level and exposure time on each tree species was analysed by 2-way ANOVA. Differences in DI, as affected by image magnification, time, and dose, were analysed by 3-way ANOVA (Table 2). Square-root transformations were used when data failed a normality test. Unless otherwise stated, significance was assumed at $P < 0.05$. All analysis was conducted using SigmaStat 3.0 (Jandel Scientific Software, San Rafael, CA, USA).

Table 2 Results of 2- and 3-way ANOVA of damage indices. Values presented are *P*-values for each effect. Please refer to the text for details of the statistical tests used

	Abaxial		Adaxial	
	High mag	Low mag	High mag	Low mag
White fir				
Day	0.431	0.158	0.786	0.254
Treatment	0.779	0.992	0.707	0.898
Day × chamber	0.210	0.736	0.918	0.636
Magnification	<0.001		0.002	
Live oak				
Day	0.311	0.100	0.014	0.514
Treatment	0.178	0.059	0.021	0.818
Day × chamber	0.711	0.618	0.644	0.995
Magnification	0.054		<0.001	
Black oak				
Day	<0.001	0.003	0.138	0.212
Treatment	0.016	0.028	0.473	0.149
Day × chamber	0.885	0.486	0.198	0.574
Magnification	0.679		0.010	
Ponderosa pine				
Day	0.036	0.038	<0.001	0.002
Treatment	<0.001	<0.001	<0.001	<0.001
Day × chamber	0.482	0.358	0.514	0.446
Magnification	0.407		0.878	

Results

Changes in the epicuticular surface; micrograph descriptions

All individuals within a species exhibited the same suite of symptoms, but the rate of response varied, even for the half-sibling oaks. Examples of the changes observed to surface features over a 32 or 33 d exposure to high levels of HNO_3 from one individual (but different leaves) are shown in Fig. 4 and 5. Fig. 4 is of ponderosa pine, and Fig. 5 is of California black oak. Both examples were captured at 1000× magnification.

Ponderosa pine. The surface of ponderosa pine needles is coated with a smooth layer of epicuticular wax, with few crystallites, except in stomatal cavities, which are filled with waxy filigree tubes (Fig. 4A). The smooth cuticle of fully expanded needles covers a corrugated-appearing subsurface. The corrugations are oriented along the long axis of the needle. After 18 d of exposure to moderate levels of HNO_3, small globular waxy formations, dubbed 'wax balls,' appeared (Fig. 4B). An electron-dense patch appeared beneath most of these structures. At 25 d, the pine needles showed severe epidermal damage (Fig. 4C). Electron-dense areas were suggestive of open lesions, and cracks parallel to the epidermal ridges were common. Wax balls were still evident at 25 d but appeared larger, more irregular and in some cases flattened. Electron-dense patches continued to be evident beneath the wax balls, but several patches had no associated waxy structure. After 32 d, the needle was highly eroded (Fig. 4D), with no changes in wax appearance in the stomatal cavities. As well, needles displayed few wax balls noted in the earlier exposures, but the wax surface appeared 'tattered' (Fig. 4D). Electron-transparent structures were evident. The exact nature and composition of these structures are not known, but if the epicuticular waxes were compromised by erosion damage, the electron-transparent features may be cellulose or cutin fibers embedded in the lower sections of the cuticle, which would be more chemically resistant to oxidation attack.[31]

California black oak. Unlike ponderosa pine, in which upper and lower leaf surfaces appear similar, the two surfaces of black

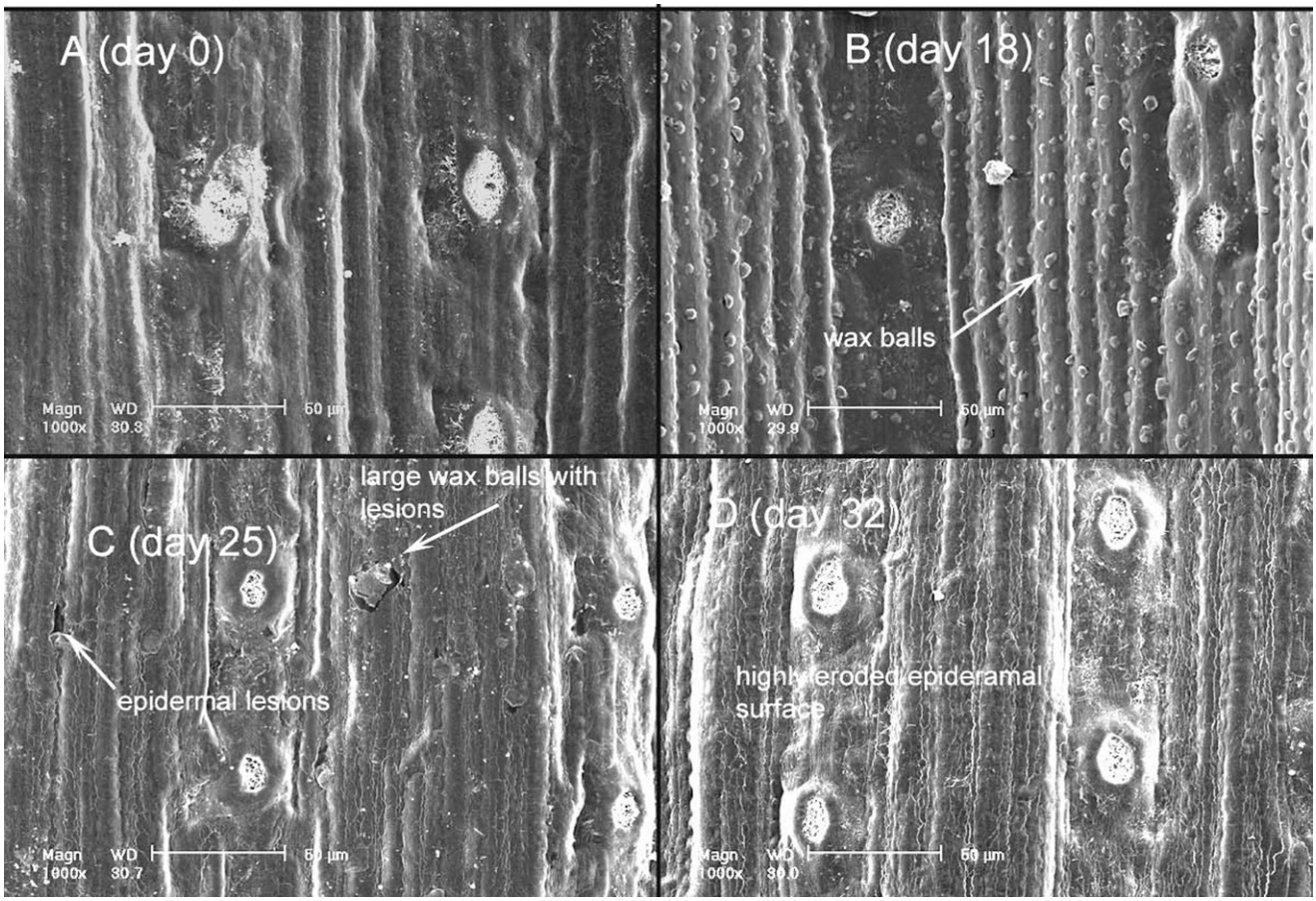

Fig. 4 Time course for development of epicuticular damage symptoms in *Pinus ponderosa*. Images are of the abaxial surface from different needles sampled from the same individual. Samples were collected from the moderate treatment chamber and images are at 1000× magnification. Panels (A)–(D): days 0, 18, 25, and 32.

oak leaves differed. Before exposure to moderate levels of HNO_3, the leaf underside was relatively smooth, with few wax balls (Fig 5A). Stellate trichomes, which are indicative of the oak family, are on both the upper and lower surface of leaves. Black oaks have a simple stomatal structure, but like ponderosa pine, the stomata are surrounded by a slightly elevated waxy ring. Before exposure, the trichome surfaces were smooth, and the outlines of epidermal cells were evident. A small amount of debris, which was not washed off prior to fumigation, was visible (Fig. 5A). Light-colored strands, perhaps cutin, were evident between stomata. After 19 d of exposure, the surface showed increased electron-light strands. Patches between stomata appeared to be collapsing and very small crystallites, analogous to the early formations of wax balls observed on pine, were scattered across the surface (Fig. 5B). After 26 d of exposure, wax balls were evident, but more widely spaced than those in pine (Fig. 5C). As well, they appeared to have electron-dense patches underneath. The trichome surface was blistered (Fig. 5C) as it was in canyon live oak (data not shown). All individuals showed this symptom, but not all images captured trichomes. At 33 d of exposure, many of the symptoms become difficult to distinguish from those of severe physical damage or aging. The originally smooth layer of wax appeared rough, with small crystallites, and small cracks, and lesions were visible. Some individuals had more lesions than others. As with ponderosa pine, black oak leaves showed no consistent pattern of damage to stomata.

Image analysis: a quantitative approach

Although each of the four species investigated exhibited different patterns in DI response, there was no interaction between day and chamber (Table 2). White fir produced no significant differences in DI values for either day or treatment relative to the controls. Image analysis indicated that the effects of HNO_3 on canyon live oak cuticles were significant only for the adaxial surface captured at high magnification. However, in both species the two levels of magnification did produce significantly different DI. Visual inspection of white fir and canyon live oak images indicated changes to the foliar surface characteristics, but these changes were not detected quantitatively by our image analysis technique.

The ability of image analysis to capture HNO_3 effects in California black oak was dependent on leaf surface. Differences in DI values were significant for day or treatment level on the abaxial surface, but not for the adaxial surface. Magnification had a significant effect on DI for the adaxial surface, but not abaxial. Ponderosa pine demonstrated significant changes in DI for all treatments, days, and for both surfaces, and those changes were captured by image analysis, regardless of the magnification.

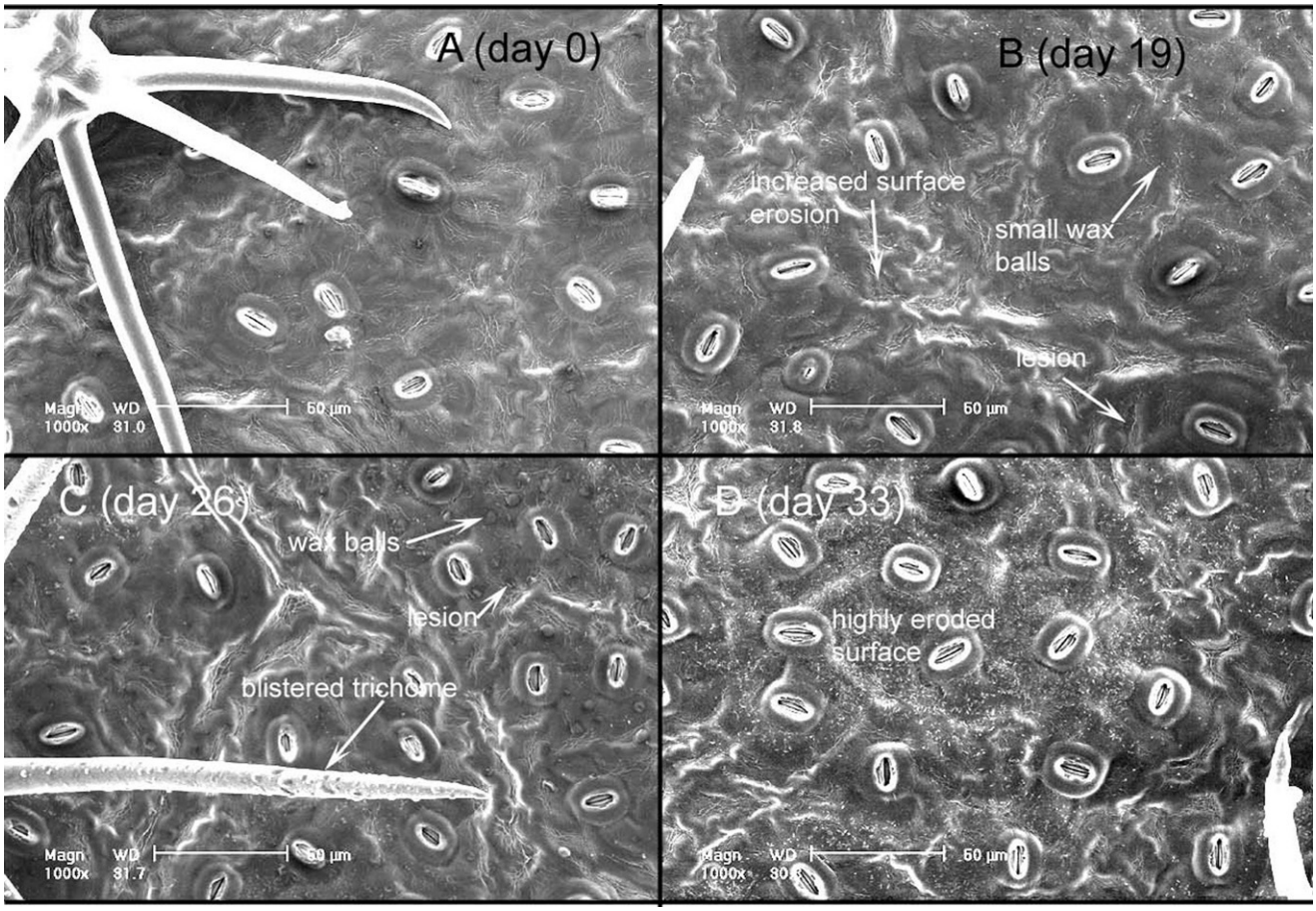

Fig. 5 Time course for development of epicuticular damage symptoms in *Quercus kelloggii*. Images are of the abaxial surface from different needles sampled from the same individual. Samples were collected from the moderate treatment chamber and images are at 1000× magnification. Panels (A)–(D): days 0, 19, 26, and 33.

Ponderosa pine. In pine, there was no difference between 1000× and 500× magnification, but a difference in DI patterns between the abaxial (Fig. 6A and B) and the adaxial (Fig. 6C and D) surfaces did emerge. On the abaxial surface, DIs reached a maximum value for the moderate treatment on day 19 and subsequently declined. The DI in the high treatment either stayed the same after day 19 (1000×) or continued to increase (500×). On the adaxial surface the DI reached a maximum of more that 4-fold greater than the initial values in the first 12 d of exposure to both treatments, followed by a significant decrease in DI. After day 19 the damage index remained nearly constant or increased slightly. For ponderosa pine, image analysis was consistent with visual inspection, but this occurrence was less the case for the other species.

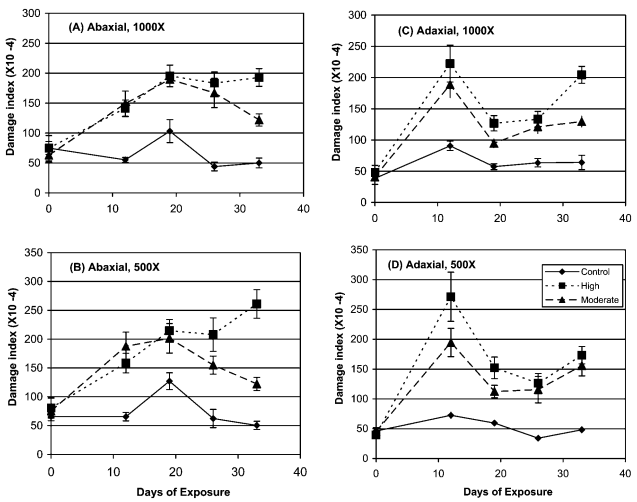

Fig. 6 Progression of damage index over exposure time in ponderosa pine. Data shown are the means of 5 samples. Error bars = σ.

Black oak. Damage indices for the abaxial surfaces (Fig. 7A and B) were 1 to 2 orders of magnitude higher than those of the adaxial surface (Fig. 7C and D). The difference in magnification was statistically significant in the adaxial surfaces, but of little practical use. The abaxial surface showed little damage until the 20th (500×) or the 27th (1000×) day. By 35 d the high and moderate treatments were statistically different from one another, and both were significantly different from the 0 HNO_3 controls.

Visible symptoms for surfaces not successfully quantified

Two different approaches to evaluating the micrographs are shown. The series of micrographs in Fig. 4 and 5 are of leaves

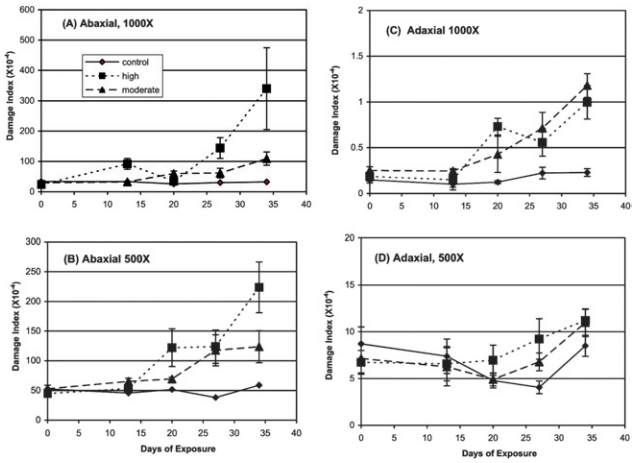

Fig. 7 Progression of damage index over exposure time in black oak. Data shown are the means of 5 samples. Error bars = σ. Note changes in y axis.

from a single individual sampled repeatedly. In Fig. 8 the micrographs are of two different individuals, one from the control chamber and one from the high-exposure chambers after 32 or 33 d of treatment. Unlike the smooth appearance of the abaxial surface, the adaxial surface of black oak is covered with scattered crystallites (Fig. 8A). After 33 d, the surface shows blistered trichomes and cracks in the epidermis. These features were difficult for NIH Image to capture, resulting in the small DI values indicated (Fig. 4A).

Canyon live oak. Fig. 8C and D show that the adaxial surface of live oak leaf surface is mostly smooth, with scattered crystallites. The density of the crystallites varied, but crystallites were present in all of the individuals investigated. Fig. 8D shows a large deformation product in the upper right-hand side of the micrograph. Many small superficial cracks are evident, with the scattered fine wax crystallites diminished in number in the same regions where the cracking was most severe. Areas of delamination are also evident. The abaxial surface of the control live oak leaf shows small waxy plates forming complicated patterns around stomata and in the interstomatal spaces (Fig. 8E). One arm of a trichome can be seen in the upper left side of the control micrograph. After 33 d the crystallites appeared melted or smeared (Fig. 8F). The possibility that this appearance might be due to handling or some other artifact was tested several times, and in all cases, the appearance was the result of HNO_3 exposure. The cuticular surface is difficult to discern beneath epicuticular crystallites, but upon careful inspection of many images, the series of cracks and lesions noted in other species were also evident in live oak.

White fir. The two surfaces of white fir (Fig. 8G and H) do not differ from one another in appearance, although like ponderosa pine, they are morphologically distinct. Both surfaces of white fir needles are covered with wax crystallites in a rosette-type formation, *cf.* ref. 21. The densities of the rosettes increases with age so that the surface becomes reflective, giving the trees a whitish sheen. Epistomatal chambers are also filled with wax crystals, similar to ponderosa pine. With increased exposure to HNO_3 vapor, the wax crystals appeared to melt together into plates or balls (Fig. 8H). Cracking appeared along the vascular ridges. In some individuals, the rosette crystalloids appeared to melt into a smear.

Types of symptoms resulting from HNO_3 exposure. Table 3 highlights the types of damage features observed, but not necessarily quantified, by image analysis. These features fell into two main categories: deformation of epicuticular crystallites and superficial wounds to the cuticle surface. It is possible that the crystallites projecting from the surface may have prevented gaseous HNO_3 from coming in contact with the surface, thus providing protection. Yet, the mechanism for both types of responses is hypothesized to be the same: chemical attack by dry deposited HNO_3.

Discussion

We have shown under controlled environmental conditions, that HNO_3 exposure produces visible symptoms of damage that results in a multiplicity of microscopic changes to leaf cuticles. The multiplicity and degree of symptoms varied among species, but were consistent within species and increased with increasing exposure.

Image analysis

Images collected by SEM can capture only a small region of the leaf surface. Whether or not a single region accurately portrays the entire surface is a concern; images collected with the intention of highlighting specific features are generally not representative. The data suggest that our protocols greatly reduced sources of bias, thus increasing the confidence that our images were indeed representative. Image editing and spatial analysis programs are becoming increasingly available and sophisticated. Through the use of these new programs, we were able to emphasize damage features, with increased contrast and false color improving the 'visibility' of these features for automated determination. Furthermore, it is now easier than ever to store and manipulate large quantities of original or edited data in a retrievable format using recordable media.

One of the accomplishments of this research was the design of a method by which digital images could be analysed through the use of spatial analysis programs. Our analysis method was, however, more effective with some species than others, and with some symptoms of damage than others. For example, the analysis of the adaxial surface of black oak was less successful than the analysis of the abaxial surface. The reason for this difference can be explained by the epicuticular microstructure. The adaxial surface of black oak leaves are covered with wax crystallites scattered across the surface (see Fig. 7A and B). These were difficult to separate from waxy granules that appeared to be caused by HNO_3. Even though damage features were visually evident and identifiable, NIH Image produced inconsistent results.

The DI was shown to be time and dose dependent. However, the appearance of symptoms and the patterns of change were complex and did not show a simple linear progression over time.

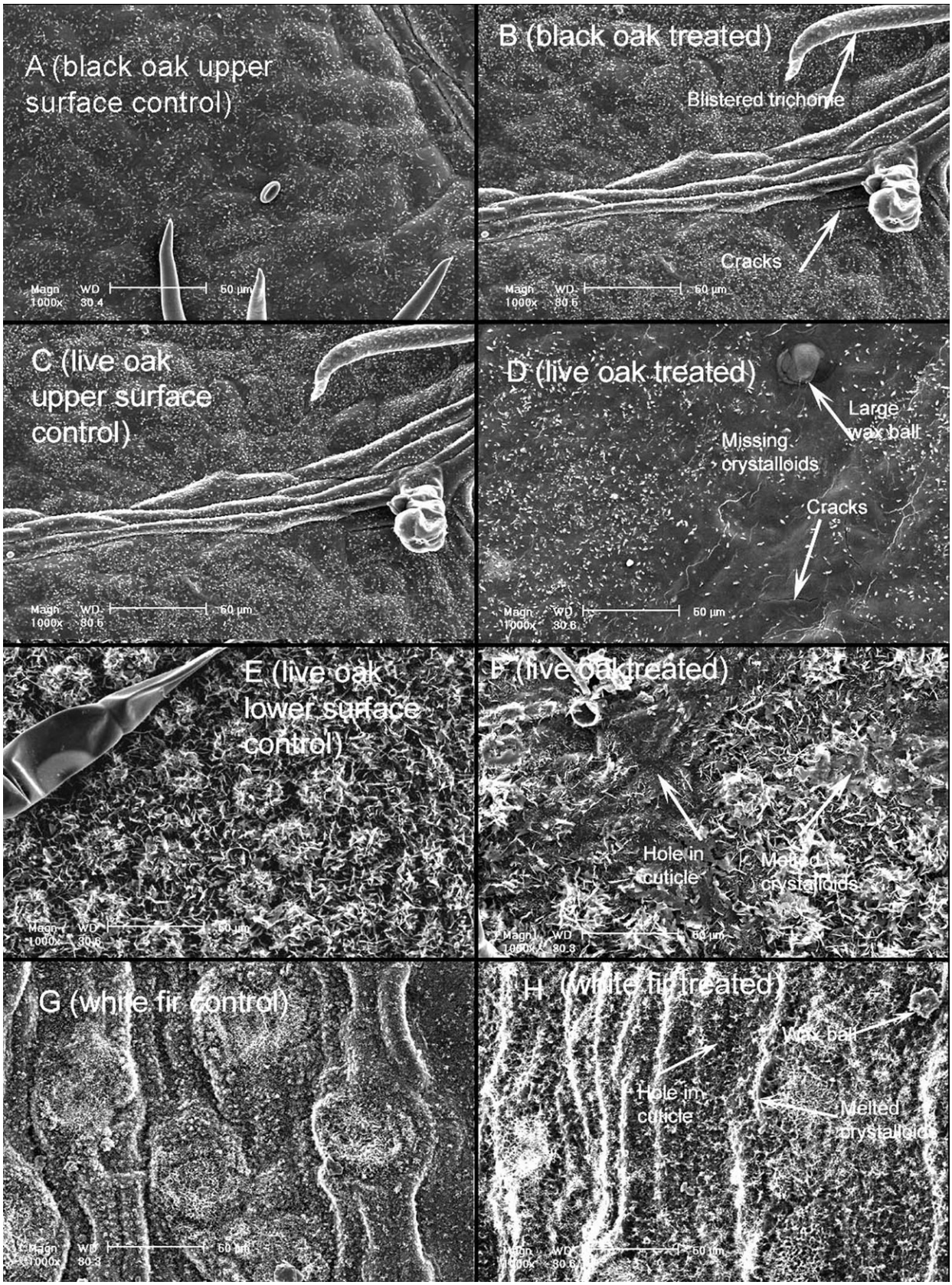

Fig. 8 Comparison of treated and control foliage after 32 or 33 days. (A) & (B) adaxial surface, black oak (*Quercus kelloggii*). (C) & (D) adaxial surface, live oak (*Quercus chrysolepis*). (E) & (F) abaxial surface, *Quercus chrysolepis*. (G) & (H) white fir (*Abies concolor*).

Table 3 Visible symptoms of damage to the leaf cuticle resulting in HNO_3 exposure

Symptom	Species	Description
Wax balls/wax blisters	Ponderosa pine, white fir, black oak, live oak	The cuticle developed a blistered appearance. Possibly a deformation of the epicuticular wax crystals. Most prominent in ponderosa pine
Cracks	Ponderosa pine, black oak, live oak	Cracks were widespread on treated leaves and appeared as fine lines, branching across the surface of the cuticle
Lesions	Ponderosa pine	Pines and oaks collected late in the experiment, demonstrated damage in the areas immediately surrounding the wax balls. Electron dense areas were also noted in the absence of deformed wax structures.
Matted or missing epicuticular wax crystals	Live oak	Live oak leaves developed irregularly shaped dark patches lacking epicuticular wax crystals. on adaxial leaf surfaces, the cuticle was often deformed in the region lacking epicuticular wax crystals.
Blistered trichome surface	Black oak, live oak	The surface of the trichomes developed a blistered appearance reminiscent of the wax balls on the cuticle.

The ponderosa pine results, for example, revealed complex features that reflected a sequence in symptoms over time. As the dose increased, the numerous small wax balls observed early during exposure appeared to have combined to form fewer but larger structures. This led to a decrease in the number of pixels counted in a 2-dimensional image, and thus a decrease in the DI, despite the quantitative increase in the amount of cuticular wax involved. Statistical analysis of white fir and three quarters of the live oak images produced no significant differences in DI, but we detected changes with visual inspection, including deformation of crystallites, wax balls, and cracking. Further research involving different magnifications, longer periods of exposure, or more samples from each individual will improve quantification of foliar response to HNO_3 deposition.

Chemical modification of cuticular surfaces

Nitric acid could cause damage to the leaf cuticle in a number of ways. Dry deposition of HNO_3 may have direct effects on the surface chemistry of the cuticle. Under laboratory conditions, aqueous HNO_3 is a strong acid and a strong oxidizing agent, both of which are capable of attacking many organic compounds.[31] Alcohols, esters, and fatty acids are significant components of leaf waxes and, at least under laboratory conditions, are subject to nucleophillic attack by NO_3^-. The structure of epicuticular wax crystals depends on their chemical composition, which is species-specific;[38,22] thus, altered chemical structure would be expected to alter the physical appearance of the epicuticular crystallites.[26]

Our operating hypothesis is that the 'wax balls' are a deformation product of chemical attack causing the smooth waxes to condense into a droplet-like form, and that the electron-dense patches are regions of highly modified or missing epicuticular waxes. With ongoing exposure, the smaller structures condense and continue to oxidize to form other products, resulting in the kinds of wax structures observed in Fig. 4C. Clearly, further chemical analysis is required to test this hypothesis.

Nitric acid may also affect the cuticle indirectly by entering the plant through a transcuticular pathway[39,40] and altering the enzyme activities responsible for wax synthesis. Many of these enzymes are known to be pH sensitive, therefore acidification of the leaf apoplast could result in modifications in synthesis processes that would changes to the chemical composition.[41,42] Although surface-deposited HNO_3 can penetrate into the mesophyll cells and be incorporated into the plant nitrogen pool through a transcuticular pathway, how this process might effect the pH balance in the mesophyll is unknown.

Environmental interactions

The effects of HNO_3 on the leaf cuticle described and quantified in this research have implications for indirect consequences of dry deposition. However, extrapolation to natural environments should be approached cautiously. The ability of HNO_3 vapor to cross the cuticular boundary has been recognized for many years.[15,43,44] However, the mechanism for transcuticular uptake of an inorganic anion has never been firmly established.[45] The data presented here strongly indicates that damage to the epicuticular wax provides ports of entry for dry deposited HNO_3. The inconsistencies among experimental results regarding the transcuticular uptake[15] could be explained by differences in dose and environmental conditions. For example, in the absence of rain, even low exposure to HNO_3 pollutants can result in dry deposition concentrations approaching that of surface saturation, typically reported in the 0.7 to 1.3 $\mu g\ cm^{-2}$ range.[44] Under these conditions chemical attack of the epicuticular wax constituents would be expected. However, exposure to very high concentrations of HNO_3 vapor would not be expected to cause damage when exposures are followed by frequent rainfall events, because surface accumulations would be washed off before critical concentrations could be reached.

If cuticular lesions caused by HNO_3 allow transcuticular uptake of NO_3^-, other gasses could cross the cuticular barrier as well. Ozone and HNO_3 are co-pollutants, because the same photochemical processes create them. Ozone is taken up exclusively by stomata during gas exchange; the permeability of cuticles to O_3 is nearly zero under environmentally relevant concentrations because it rapidly decomposes when crossing the epicuticular boundary.[46] Therefore, when stomata are closed during drought stress, O_3 is excluded from the foliar apoplast. In the western yellow pines, chlorotic mottle is a well-established symptom of O_3 toxicity. Since the highest O_3 concentrations in southern California correspond to the droughty summer months, the ability of O_3 to incur damage when stomata are generally closed has been difficult to explain.[6,47] Lesions caused by HNO_3 attack would provide an alternative pathway for O_3 penetration

into the leaf's interior. Although this study could not establish whether cuticular damage left epidermal cells exposed, clearly a large reduction in the protective epicuticular barrier would leave epidermal cells more vulnerable to O_3 toxicity.

Conclusion

Air pollution will continue to be an issue in the future as human populations continue to expand and urbanization encroaches on wild lands. The effects of air pollution are often subtle and cumulative, and they are additive to other stresses that are a natural part of the ecological life cycle. Establishing the mechanisms and causes and effects of individual components of air pollution is a critical first step in understanding the complicated interactions among biotic and abiotic factors that shape ecological processes

Acknowledgements

This work was funded by a grant from USDA-NRI (#970163). We thank Dr Krassimir Bozhilov at the Electron Microscopy Facility, UCR, for his assistance and guidance in preparing samples for SEM; Dr George Riechers for the initial design of the fumigation system; Dr Kevin Percy, Canadian Forest Service, for initiating the preliminary studies that were the foundation of this work; and Laura Heraty for editorial assistance.

References

1 J. H. Seinfeld and S. N. Pandis. *Atmospheric Chemistry and Physics: From Air Pollution to Climate Change*, John Wiley & Sons, Inc, New York, USA, 2nd edn, 2005.
2 H. Furutani and H. Akimoto, Development and characterization of a fast measurement system for gas-phase nitric acid with a chemical ionization mass spectrometer in the marine boundary layer, *J. Geophys. Res.*, 2002, **107**(D2), DOI: 10.1029/2000JD000269.
3 M. Possanzini, A. Febo and A. Liberti, New design of a high performance denuder for the sampling of atmospheric pollutants, *Atmos. Environ.*, 1983, **17**, 2605–2610.
4 J. Slanina, P. J. de Wild and G. P. Wyers, The application of denuder systems to the analysis of atmospheric components, in *Gaseous Pollutants: Characterization and Cycling*, ed. J. O. Nriagu, John Wiley & Sons, Inc., New York, USA, 1992, pp. 129–154.
5 H. Müller, G. Kramm, F. Meixner, G. J. Dolard, D. Fowler and M. Possanzini, Determination of HNO_3 dry deposition by modified Bowen ration and aerodynamic profile techniques, *Tellus*, 1993, **45B**, 346–367.
6 A. Bytnerowicz, Physiological/ecological interactions between ozone and nitrogen deposition in forest ecosystems, *Phyton*, 2002, **42**, 13–28.
7 NADP, Nitrogen in the Nation's Rain, *National Atmospheric Deposition Program Brochure 2000–01a*, Champagne, IL, 2000.
8 M. E. Fenn, M. A. Poth, S. L. Schilling and D. B. Grainger, Throughfall and fog deposition of nitrogen and sulfur at an N-limited and N-saturated site in the San Bernardino Mountains, southern California, *Can. J. For. Res.*, 2000, **30**, 1479–1488.
9 A. Bytnerowicz and M. E. Fenn, Nitrogen deposition in California forests: a review, *Environ. Pollut.*, 1996, **92**, 127–146.
10 P. E. Padgett, E. B. Allen, A. Bytnerowicz and R. A. Minnich, Changes in soil inorganic nitrogen as related to atmospheric nitrogenous pollutants in southern California, *Atmos. Environ.*, 1999, **33**, 769–781.
11 S. H. Cadle, J. M. Dasch and P. A. Mulawa, Atmospheric concentrations and the deposition velocity to snow of nitric acid, sulfur dioxide and various particulate species, *Atmos. Environ.*, 1985, **19**, 1819–1827.
12 G. M. Lovett, Atmospheric deposition of nutrients and pollutants in North America: An ecological perspective, *Ecol. Appl.*, 1994, **4**, 629–650.
13 M. E. Fenn and A. Bytnerowicz, Summer throughfall and winter deposition in the San Bernardino Mountains in southern California, *Atmos. Environ.*, 1997, **31**, 673–683.
14 T.-C Lin, S. P. Hamburg, H.-B. King and Y.-J. Hsia, Throughfall patterns in a subtropical rain forest of northeastern Taiwan, *J. Environ. Qual.*, 2000, **29**, 1186–1193.
15 S. Nussbaum, M. Ammann and J. Fuhrer, Foliar absorption and use of airborne oxidized nitrogen by terrestrial plants, in *Nitrogen Nutrition and Plant Growth*, ed. H. S. Srivastava and R. P. Singh, Science Publisher, Inc., Enfield, NH, USA, 1999, pp. 103–172.
16 A. Bytnerowicz, K. Percy, G. Riechers, P. Padgett and M. Krywult, Nitric acid vapor effects on forest trees – deposition and cuticular changes, *Chemosphere*, 1998, **36**, 697–702.
17 M. Krywult, J. Hom, A. Bytnerowicz and K. E. Percy, Deposition of gaseous nitric acid and its effects on foliage of ponderosa pine (*Pinus ponderosa* Dougl. Ex Laws.) seedlings, in *IUFRO Air Pollution and Multiple Stresses*, ed. R. Cox, K. Percy, K. Jensen and C. Simpson, Canadian Forest Service, Fredericton, CA, 1996, pp. 45–51.
18 P. E. Padgett, A. Bytnerowicz, P. J. Dawson, G. H. Riechers and D. R. Fitz, Design, evaluation and application of a continuously stirred tank reactor system for use in nitric acid air pollution studies, *Water, Air, Soil Pollut.*, 2004, **151**, 35–51.
19 J. N. Cape and K. E. Percy, Environmental influences on the development of spruce needle cuticles, *New Phytol.*, 1993, **125**, 787–799.
20 B. Prügel, P. Loosveldt and J.-P. Garrec, Changes in the content and constituentsof the cuticular wax of *Picea abies* (L.) Karst. in relation to needle ageing and tree decline in five European forest areas, *Trees*, 1994, **9**, 80–87.
21 W. Barthlott, C. Neinhuis, D. Cutler, R. Ditsch, I. Meusel, I. Theisen and H. Wilhelmi, Classification and terminology of plant epicuticular waxes, *Bot. J. Linn. Soc.*, 1998, **126**, 237–260.
22 D. Post-Beittenmiller, Biochemistry and molecular biology of wax production in plants, *Annu. Rev.Plant Physiol. Plant Mol. Biol.*, 1996, **47**, 405–430.
23 M. Riederer and C. Markstädter, Cuticular waxes: a critical assessment of current knowledge, in *Plant Cuticles*, ed. G. Kerstiens, Oxford, UK, BIOS Scientific Publishers, 1996, pp. 189–200.
24 L. Kunst and A. L. Samuels, Biosynthesis and secretion of plant cuticular wax, *Progr. Lipid Res.*, 2003, **42**, 51–80.
25 K. E. Percy and E. A. Baker, Effects of simulated acid rain on epicuticular wax production, morphology, chemical composition and on cuticular membrane thickness in two clones of Sitka spruce [*Picea sitchensis* (Bong.) Carr.], *New Phytol.*, 1990, **116**, 79–87.
26 M. Turunen and S. Huttunen, A review of the response of epicuticular wax of conifer needles to air pollution, *J. Environ. Qual.*, 1990, **19**, 35–45.
27 A. Bytnerowicz and N. E. Grulke, Physiological effects of air pollutants on western trees, in *The Response of Western Forests to Air Pollution*, ed. R. K. Olson, D. Binkley and M. Bohm, Springer-Verlag, New York, USA, 1992, pp. 183–233.
28 K. E. Percy, K. F. Jensen and C. J. McQuattie, Effects of ozone and acidic fog on red spruce needle epicuticular wax production, chemical composition, cuticular membrane ultrastructure and needle wettability, *New Phytol.*, 1992, **122**, 71–80.
29 C. Trimbacher and P. Weiss, Needle surface characteristics and element contents of Norway spruce in relation to the distance of emission sources, *Environ. Pollut.*, 1999, **105**, 111–119.
30 L. E-Viskari, Epicuticular wax of Norway spruce needles as an indicator of traffic pollutant deposition, *Water, Air, Soil Pollut.*, 2000, **121**, 327–337.
31 M. Hudlicky, *Oxidations in Organic Chemistry*, ACS Monograph 186, American Chemical Society, Washington, DC, USA, 1990.
32 C. E. Jeffree, E. A. Baker and P. J. Holloway, Ultrastructure and recrystallization of plant epicuticular waxes, *New Phytol.*, 1975, **75**, 539–549.
33 I. Meusel, C. Neinhuis, C. Markstädter and W. Barthlott, Ultrastructure, chemical composition, and recrystallization of epicuticular waxes: transversely ridged rodlets, *Can. J. Bot.*, 1999, **77**, 706–720.
34 K. E. Percy, C. S. Awmack, R. I. Lindroth, M. E. Kubiske, B. J. Kopper, J. G. Isebrands, K. S. Pregitzer, G. R. Hendrey, R. E. Dickson, D. R. Zak, E. Oksanen, J. Sober, R. Harrington

and D. F. Karnosky, Altered performance of forest pests under CO_2^- and O_3-enriched atmospheres, *Nature*, 2002, **420**, 403–407.
35 C. Trimbacher and O. Echmüllner, A method of quantifying changes in the epicuticular wax structure of Norway spruce needles, *Eur. J. For. Pathol.*, 1997, **27**, 83–93.
36 B. M Pavlic, P. C. Muick, S. G. Johnson and M. Popper, *Oaks of California*, Cachuma Press, Olivos, CA, USA, 1991, 184 pp.
37 A. S. Heagle and R. B. Philbeck, Exposure Techniques, in *Proceedings: A Special Conference on Methodology for the Assessment of Air Pollution Effects on Vegetation*, ed. W. W. Heck, S. V. Krupaand S. N. Linzon, 1979, pp. 6-1–6-19.
38 P. J. Holloway, Plant cuticles: physiochemical characteristics and biosynthesis, in *Air Pollutants and the Leaf Cuticle*, ed. K. E. Percy, J. N. Cape, R. Jagels and C. J. Simpson, NATO ASI Series G, Springer Verlag, Berlin, Germany, 1994, vol. 36, pp. 1–14.
39 J. D. Marshall and S. H. Cadle, Evidence of trans-cuticular uptake of HNO_3 vapor by foliage of eastern white pine (*Pinus strobus* L.), *Environ. Pollut.*, 1989, **60**, 15–28.
40 P. J. Hanson and C. T. Garten, Deposition of $H^{15}NO_3$ vapor to white oak, red maple and loblolly pine foliage: experimental observations and a generalized model, *New Phytol.*, 1992, **122**, 329–337.
41 K. E. Percy, C. J. McQuattie and J. A. Rebbeck, Effects of air pollutants on epicuticular wax composition, in *Air Pollutants and the Leaf Cuticle*, ed. K. E. Percy, J. N. Cape, R. Jagel and C. M. Simpson, NATO ASI series, Springer-Verlag, Berlin Deu, 1994, vol. 36, pp. 67–79.
42 S. Huttunen, Effects of air pollutants on epicuticular wax structure, in *Air Pollutants and the Leaf Cuticle*, ed. K. E. Percy, J. N. Cape, R. Jagels and C. M Simpson, NATO ASI series Vol. G36, Springer-Verlag, Berlin, Deu, 1994, vol. 37, pp. 81–96.
43 R. J. Norby, Y. Weerasuriya and P. J. Hanson, Induction of nitrate reductase activity in red spruce needles by NO_2 and HNO_3 vapor, *Can. J. For. Res.*, 1989, **19**, 889–896.
44 S. H. Cadle, J. D. Marshall and P. A. Mulawa, A laboratory investigation of the routes of HNO_3 dry deposition to coniferous seedlings, *Environ. Pollut.*, 1991, **72**, 287–305.
45 M. Riederer and L. Schreiber, Waxes – the transport barriers of plant cuticles, in ed. R. J. Hamilton, *Waxes: Chemistry, Molecular Biology and Functions*, the Oily Press Ltd., Dundee Scotland, UK, 1996, pp. 131–156.
46 G. Kerstiens, *Diffusion of Water Vapour and Gases across Cuticles and through Stomatal Pores Presumed Closed*, in *Plant Cuticles*, ed. G. Kerstiens, BIOS Scientific Publishers, Oxford, UK, 1996, pp. 121–134.
47 N. E. Grulke, R. Alonso, T. Nguyen, C. Cascio and W. Dobrowolski, Stomata open at night: implications for pollutant uptake in ponderosa pine, *Tree Physiol.*, 2004, **24**, 1001–1010.
48 C. Potvin, ANOVA: Experiments in controlled environments, in *Design and Analysis of Ecological Experiments*, ed. S. M. Scheiner and J. Gurevitch, Chapman & Hall, New York. 1993 pp. 48–68.
49 R. C. Musselman and B. A. Hale, Methods for controlled and field ozone exposures of forest species, in *Forest Decline and Ozone: A Comparison of Controlled Chamber and Field Experiments*, ed. H. Sandermann, A. R. Wellburn and R. L. Heath, *Q. Rev. Biol.*, 1997, **72**(4), 277–315.

